Polymer Testing 29 (2010) 7–13

Contents lists available at ScienceDirect

Polymer Testing

journal homepage: www.elsevier.com/locate/polytest

Property Modelling

Strain distribution in cruciform specimens subjected to biaxial loading conditions. Part 1: Two-dimensional versus three-dimensional finite element model

Ebrahim Lamkanfi [a,*], Wim Van Paepegem [a], Joris Degrieck [a], Carla Ramault [b], Andreas Makris [b], Danny Van Hemelrijck [b]

[a] Department of Materials Science and Engineering, Ghent University, Sint-Pietersnieuwstraat 41, 9000 Ghent, Belgium
[b] Department of Mechanics of Materials and Constructions, Free University of Brussels, Pleinlaan 2, 1050 Brussels, Belgium

ARTICLE INFO

Article history:
Received 16 July 2009
Accepted 26 August 2009

Keywords:
Laminate
Strength
Stress concentrations
Finite element analysis
Biaxial

ABSTRACT

The current study discusses the importance of sufficiently detailed finite element models in the understanding of failure mechanisms in biaxially loaded cruciform specimens. It is shown that the development of two-dimensional models can only be reliable outside the region of geometrical discontinuities such as the fillet corners and the milled centre zone. A comparison with experimentally obtained surface strains, by means of the digital image correlation technique, showed a large mismatch in these regions. However, a more detailed three-dimensional approach proved that this mismatch in strain values between the numerical and experimental results could only be due to a miscorrelation in the digital image correlation images. This conclusion revealed the existence of a crack at the transition zone between the milled and un-milled area, which could only be found due to the more detailed approach of the three-dimensional finite element model.

1. Introduction

Material characterization is in general not an easy task, especially so in the case of composite materials. Researchers have tried for many years to develop constitutive relations and failure criteria to make more widespread use of these materials in different industrial sectors possible. Unfortunately, the current practice of using uniaxial tests as a basis for failure prediction of these inhomogeneous and anisotropic materials under multiaxial stress states has proven to be insufficient. Therefore, biaxial and multiaxial tests appeared necessary to improve our understanding in the mechanical behavior of these complex materials. During recent decades, many different test set-ups have been used to produce biaxial stress states: anticlastic bending tests of rhomboidal composite plates [1–5], thin-walled tubes subjected to a combination of axial loading, torsion and internal/external pressure [6–8] and cruciform specimens under in-plane biaxial loading [9–13] are just a few from a wide variety of testing techniques. Although in theory these tests should give a significant improvement of our knowledge in this matter, practically it was found that it is not an easy task to perform them. Conditions such as the start of failure being in the biaxially loaded test zone or the capability to perform various biaxial stress/strain ratios, and also the requirement that a uniform strain distribution is obtained in the biaxially loaded zone, complicate the achievement of reliable results. To overcome these problems, the development of numerical models can significantly improve our understanding in many of these difficulties. However, due to complex material behavior, large differences in numerical results can be obtained depending on the chosen level of

* Corresponding author. Tel.: +32 9 264 95 34.
E-mail addresses: ebrahim.lamkanfi@ugent.be, elamkanf@gmail.com (E. Lamkanfi).

0142-9418/$ – see front matter © 2009 Elsevier Ltd. All rights reserved.
doi:10.1016/j.polymertesting.2009.08.009

modeling. In this regard, a comparison between a two-dimensional and a full three-dimensional finite element model of a biaxially loaded cruciform specimen is presented. Besides the similarities found between these two approaches, also the most important shortcomings are discussed. Moreover, a validation of the numerically obtained surface strains by means of the digital image correlation technique is also shown.

2. Cruciform geometry

The present geometry discussed here has been developed in the European Optimat Blades project [14] where a broad study was performed on the construction of rotor blades used in the wind turbine industry. The material investigated in this project was a glass fibre reinforced plastic (GFRP) manufactured by LM Glasfiber using RTM technology. The $[(\pm 45^\circ/0^\circ)_4/\pm 45^\circ]$ stacking sequence of this material (Fig. 1), with the $[0^\circ]$ layers aligned along the x-direction of the global coordinate system in Fig. 2, is balanced due to the internal symmetry of the $[\pm 45^\circ]$ plies. The dimensions of the specimen are depicted in the right part of Fig. 1. The arms have a width of 25 mm and a total length of 250 mm in the two directions. The thickness of the $[0^\circ]$ layers is 0.88 mm, whereas the $[+45^\circ]$ and $[-45^\circ]$ layers have an equal thickness of 0.305 mm. As one can observe in Fig. 2, each of the four corners has been cut out with two rounding radii: an inner radius of 25 mm and a outer radius, nearer to the centre, of 12.5 mm. The intention of these cut-outs lies in the prevention of a direct transfer of loads from the horizontal arms to the vertical ones due to the dominant presence of $[\pm 45^\circ]$ layers in the stacking sequence. Failing to meet this requirement will lead to a high concentration of shear stresses in the corner zones, ending up in premature failure. A second type of discontinuity can be found in the centre area of the laminate where one group of $[\pm 45^\circ/0^\circ]$ at each side of the specimen, is milled away. This results in a gradual decrease of the total thickness of 6.57 mm in the arms (zone A) to a thickness of 3.59 mm in the central area (zone B) along

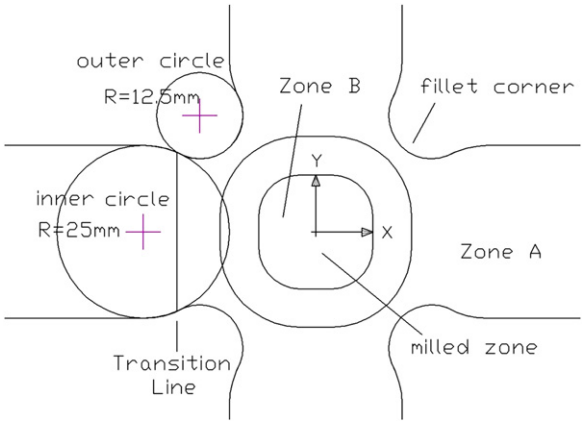

Fig. 2. Radii at the fillet corner and the milled zone.

a 15° skew edge with the horizontal (Figs. 1 and 2). This reduction in thickness appears to be necessary to prevent premature breakage in the arms. This can be understood from the fact that the centre zone has a greater capacity to endure a larger stress state because of its biaxial strength compared with that of the arms.

One of the disadvantages of this complex geometry is that the relation between the externally applied loads in the arms of the cruciform specimen and the resulting stress field in the centre of the specimen cannot be determined in an analytical way. Even the use of experimental measuring techniques, such as strain gauges or extensometers, is not sufficient because of the averaged value of the deformation along their gauge length. Therefore, the digital image correlation technique (DICT) is used as a more precise experimental method to measure the surface strain distribution of the biaxially loaded centre.

3. Digital image correlation

Optical techniques such as moiré interferometry [15], holography [16] and speckle interferometry [17] have

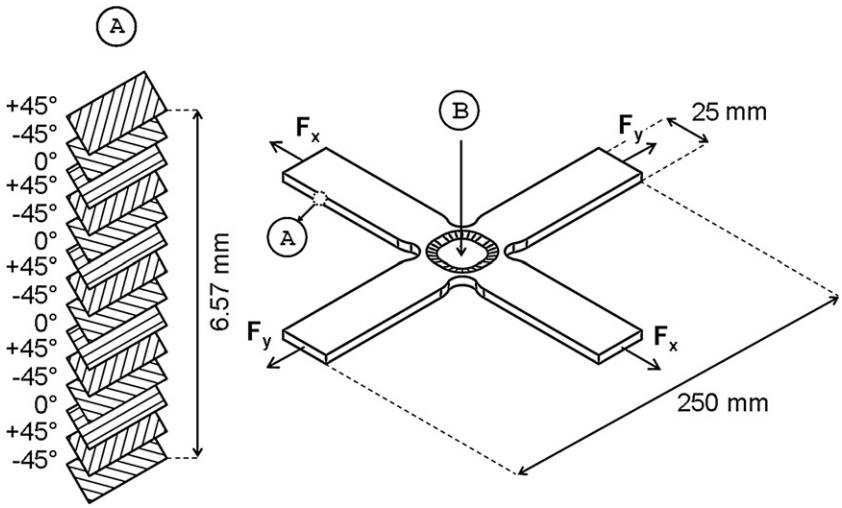

Fig. 1. Stacking sequence (left) and cruciform dimensions (right).

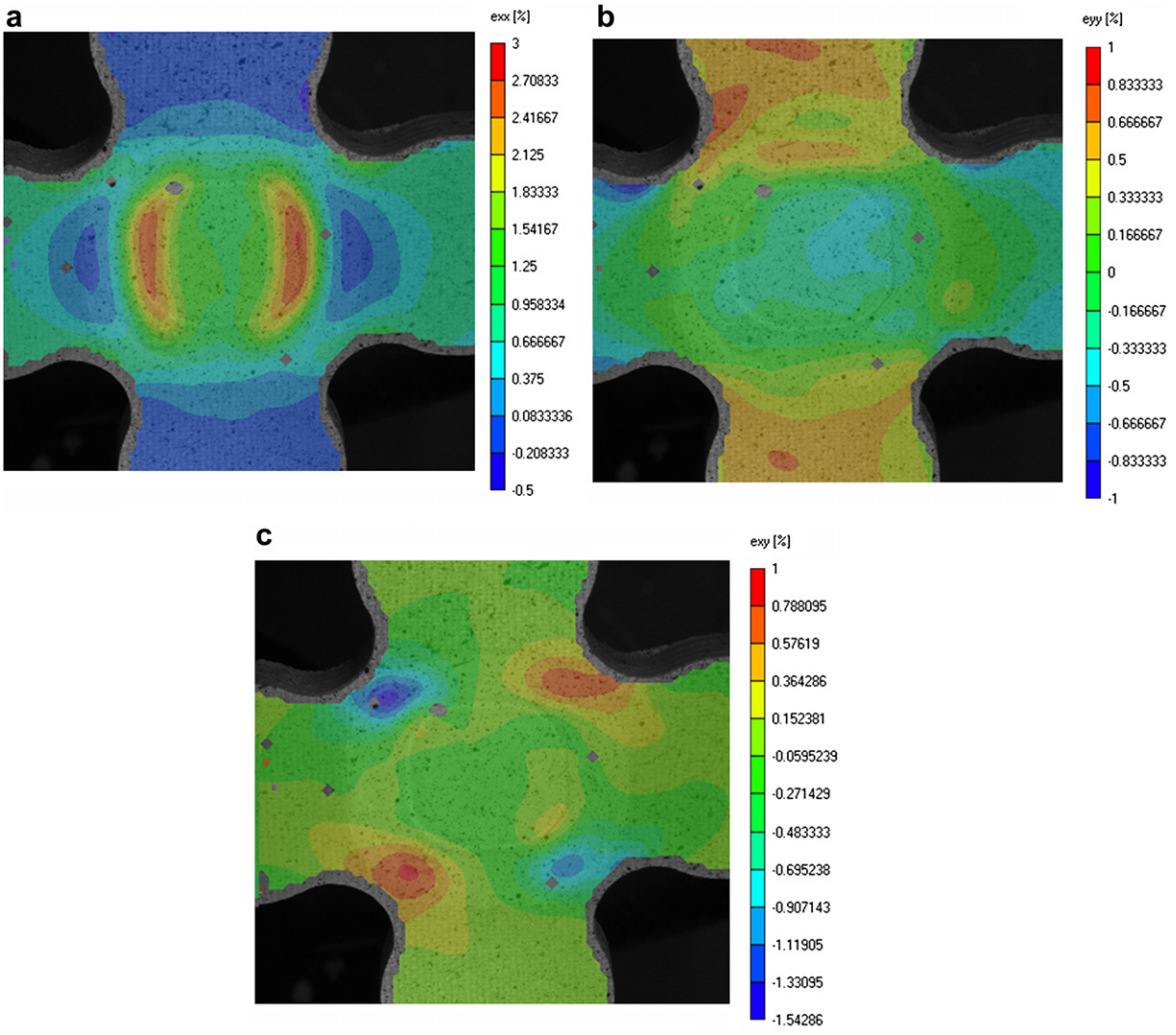

Fig. 3. Strains ε_{xx} (a), ε_{yy} (b) and ε_{xy} (c) on the surface of a biaxially loaded specimen obtained with the DICT. Biaxial Load at 80% of the ultimate load.

become increasingly important in measuring displacements and displacement gradients. Also, the digital image correlation technique has attracted the necessary attention of many researchers. Especially, its direct sensing capability and the exclusion of any laborious and time-consuming fringe pattern processing made it a very attractive method in comparison with the ones mentioned above. In the current paper, this non-contacting optical method will be used for the full field measuring of strains. The essence of this technique lies in the comparison of surface images taken at different loading steps. After application of a random speckle pattern onto the surface of the cruciform, a charge couple device camera captures images from the area of interest in the un-deformed and deformed states. The gathered high resolution images are digitized and a correlation algorithm is then employed to find the sub-pixel displacements between successive pictures. Once these deformations are obtained, the spatial derivative is applied to calculate the surface strains.

In Fig. 3a–c, the strains ε_{xx}, ε_{yy} and ε_{xy} are respectively shown along the two orthogonal axes as an example of this method. It can be clearly seen that the accuracy of the results depends on the quality of the speckle pattern. In the zones where the surface treatment has a low quality, i.e. the speckle pattern is disturbed by large speckles, no correlation can be found between the points which results

Table 1
Material characteristics for glass fibre reinforced epoxy.

E_{11} [GPa]	39.10
E_{22} [GPa]	14.44
E_{33} [GPa]	14.44
ν_{12} [–]	0.294
ν_{13} [–]	0.294
ν_{23} [–]	0.294
G_{12} [GPa]	5.39
G_{13} [GPa]	5.39
G_{23} [GPa]	5.39

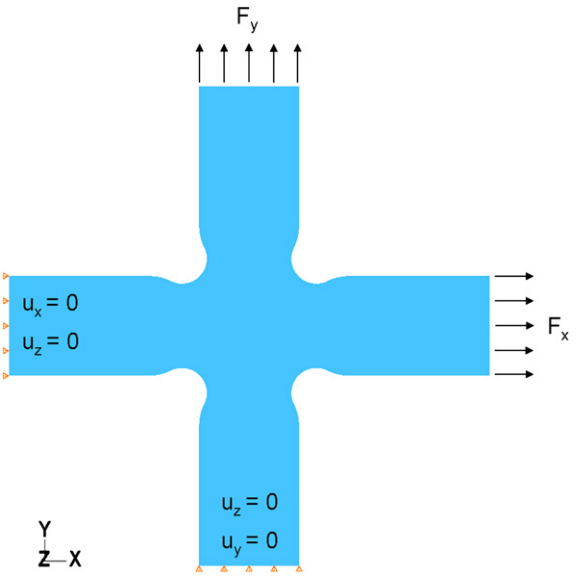

Fig. 4. Applied loads and boundary conditions to the 2D model.

in "dead pixel values" (left arm of Fig. 3a and b). During the experiments, it appeared that only trial and error attempts can provide the necessary experience to obtain sufficiently accurate results. One can also observe on Fig. 3a and b that the border regions remain totally uncorrelated and, therefore, no strains are visible in those zones. Though these regions remain unknown with the DIC technique, it will be shown in the next paragraphs by application of the finite element method that the stresses and strains in these borders reach very high values and, therefore, play an important role in understanding the failure mechanisms. At this moment we will try to focus on the area of the cruciform where reliable correlations are obtained in order to derive the strain fields.

Throughout this study, the biaxial load ratio is maintained at 3.85, leading to a final failure of the specimen at average load values of 46.2 kN in the *x*-direction and 12 kN in the *y*-direction. Regardless of the fact that a uniaxial (in the *x*- or the *y*-direction) or a biaxial load is applied, the horizontal axis is always the direction of the highest load.

4. Finite element model

The finite element method (FEM) is employed in this paper as a detailed method for the study of the strain distribution of the cruciform. In a first stage, a simplified two-dimensional model will enable us to have a preliminary comparison with the surface strain fields obtained by the digital image correlation technique. Also, a more accurate 3D numerical model has been developed to help us understand how the loads and strains are distributed over the central area. Moreover, this detailed approach will also highlight the shortcomings and the usefulness of the two-dimensional model leading to the acceptance or denial of the computationally less expensive 2D models. For this purpose, the commercial FEM package ABAQUS^{TM} was used.

The 2D and the 3D numerical models are built up with the same geometry, stacking sequence, boundary conditions and material characteristics (Table 1). In the case of the 2D shell model, the lamina stresses for the composite cruciform subjected to a biaxial in-plane force are determined by using the classical lamination theory where a homogenization of the material parameters is employed. This implies that although no physical layers are modeled, the contribution of each layer is still taken into account in the global stiffness matrix. Therefore, it is made possible to obtain, besides the averaged stresses and strains for the entire model, also the results in each individual layer. However, the fact that the inter-laminar stresses and the through thickness stresses in the layers are themselves neglected, is a major drawback of this modeling technique.

The boundary conditions used in this model are depicted in Fig. 4 where the displacements are locked in specific directions. At the left edge of the horizontal arm, no displacement in the *x*-direction is accepted, whereas the transverse cross section/movement is allowed to deform freely. A similar condition is applied at the lower edge of the vertical arm: the displacement in the *y*-direction is fixed whereas the one in the *x*-direction is allowed. Furthermore, the four ends of the arms are also prevented from moving in the *z*-direction. The loads are also shown in Fig. 4. It is obvious that the results obtained by use of this 2D formulation can only be the in-plane components of the full 3D stress and strain tensors. For the three-dimensional model, each layer in the composite is modeled with solid elements as an independent layer which is constrained with a tie to its surrounding layers.

4.1. Two-dimensional model

Before trying to simulate the more complex 3D model, a reproduction of DIC images with a two-dimensional model is desirable to prove the feasibility of the finite element method. In this model, the largest edge load in the *x*-direction has a magnitude of 1848 N/mm which corresponds to the 46.2 kN mentioned above (F_x in Fig. 4), whereas the load in the *y*-direction is a factor 3.85 lower. For the discretization, two-dimensional S4R shell elements with 4 degrees of freedom and with the reduced integration scheme have been chosen. For completeness, it also mentioned that the skew edges of the milled zone are approximated by the use of cylindrical cut-outs which bound the milled zone with vertical edges. The outcome of the calculations can be found in Fig. 5a–c where, respectively, the strains ε_{xx}, ε_{yy} and γ_{xy} are shown in the global coordinate system. These figures can be compared with those in Fig. 3. One has to give attention to the shear strains, because they are expressed in the DIC method as ε_{xy}, whereas in the finite element model the engineering strains $\gamma_{xy} = 2\varepsilon_{xy}$ are used. From Fig. 5b and c, it can be clearly seen that the strains ε_{yy} and $\gamma_{xy}/2$ agree very well with the corresponding ones obtained with DIC technique (Fig. 3b and c). However, for the ε_{xx} strains a large difference can be found between Figs. 3a and 5a, where a maximum value of 3% is observed in the biaxial zone with the experimental method, whereas the FEM method only predicts a maximum 1.3% strain value in that region. This

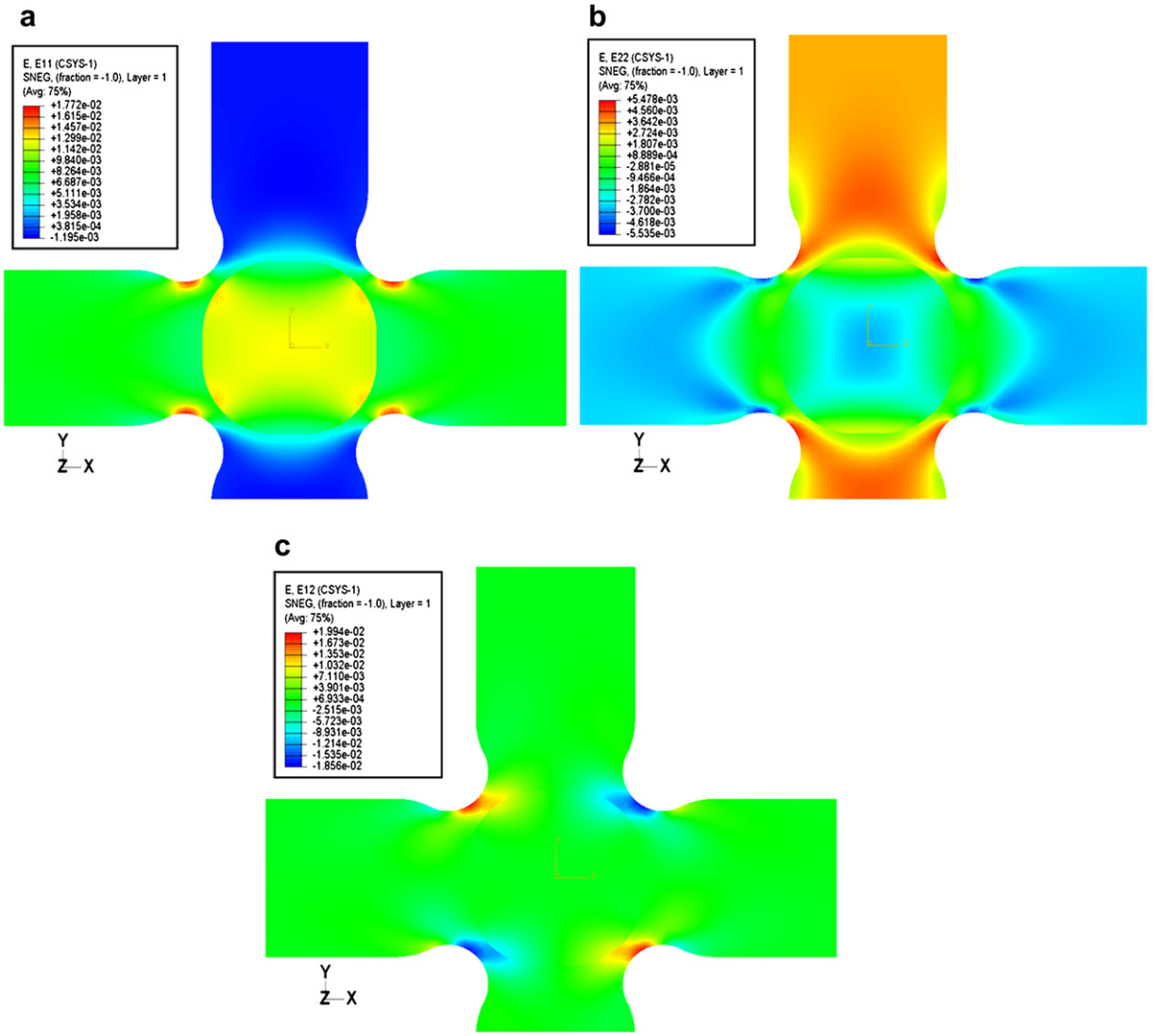

Fig. 5. Strains ε_{xx} (a), ε_{yy} (b) and γ_{xy} (c) in the global coordinate system for the 2D model. Biaxial applied load is taken at 80% of the ultimate load.

mismatch can be explained by taking the simplifications of the two-dimensional model into account as well as the approximate modeling of the milled zone. The three-dimensional model has to solve these inadequacies.

4.2. Three-dimensional model

For the three-dimensional situation, the same simulation as the two-dimensional one was conducted with regard to the lay-up, loads and boundary conditions. For the type of elements, the 8 node brick continuum elements with the reduced integration scheme have been considered. The results can be found in Fig. 6a–c. It appears that the surface strains are corresponding fairly well with the 2D ones, especially in the arms of the specimen. This observation justifies the shortening of the arms which leads to a smaller and computationally more efficient model in the following paragraphs. Also, the results from the layers different from the surface ones correspond very well with those of the 2D model. This is can be seen for example in Fig. 7a where the ε_{xx} strains are depicted in the first un-milled [+45°] layer in the 2D model and in Fig. 7b for the corresponding results in the 3D model. However, a closer look at the milled zone in Fig. 8a reveals an anomaly for this cross-shaped specimen. Although the digital image correlation technique and the finite element method capture the same ε_{xx} strain pattern in the milled zone, the magnitudes remain much higher (3%) in this area for the DIC method (Fig. 3a) compared with those found in the numerical simulation of Fig. 6a (1.318%), particularly at the transition zone between the skew edges and the milled area. In this zone, these strain intensities ε_{xx} exhibit a specific "half moon" pattern, which is given the name "half moon" due to the shape of the intensity zone. Moreover, when a closer look is taken at the DIC images, a crack is observed in this region (Fig. 8) which is responsible for

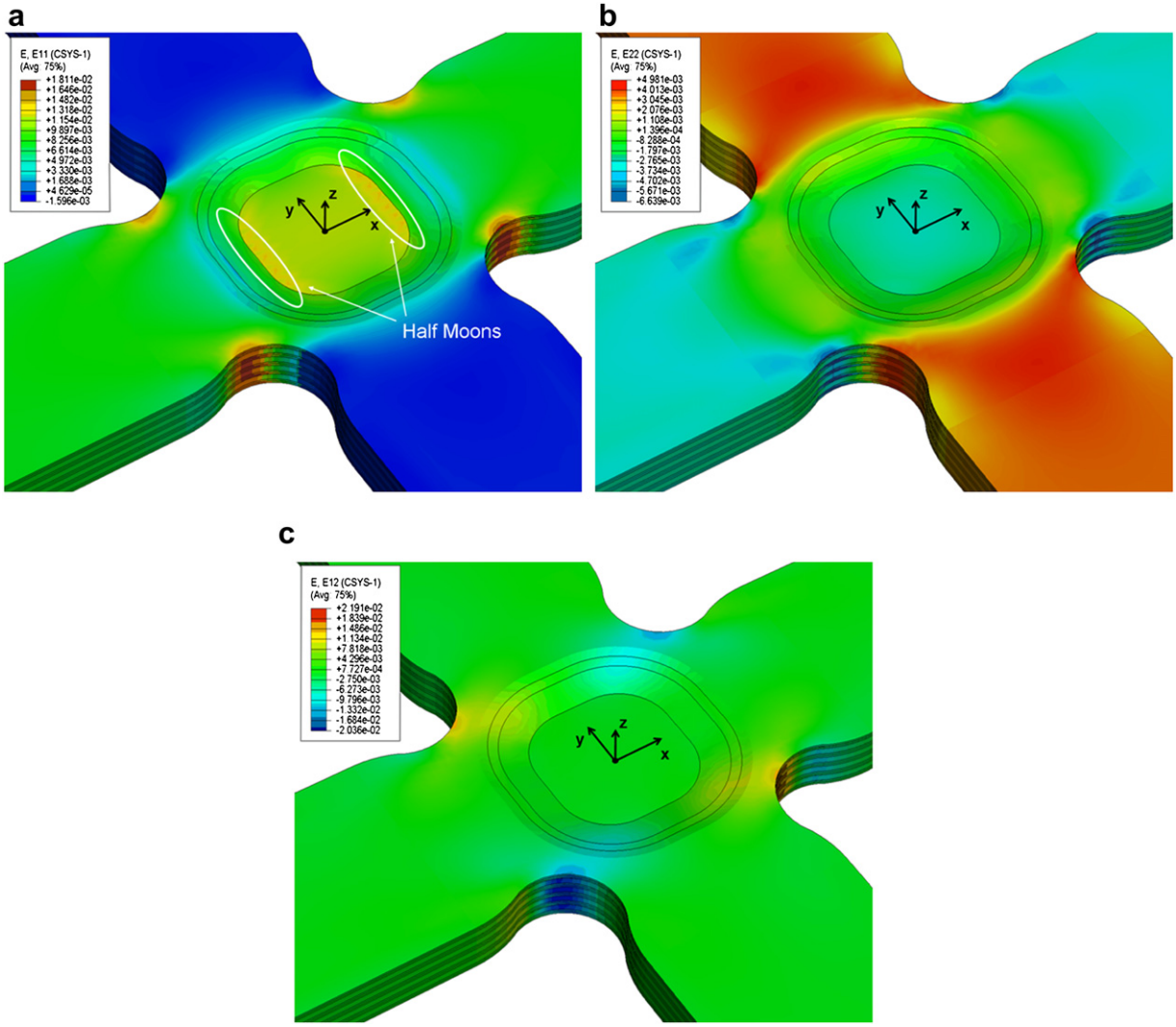

Fig. 6. Strains ε_{xx} (a), ε_{yy} (b) and ε_{xy} (c) in the global coordinate system for the 3D model. Biaxial applied load is taken at 80% of the ultimate load.

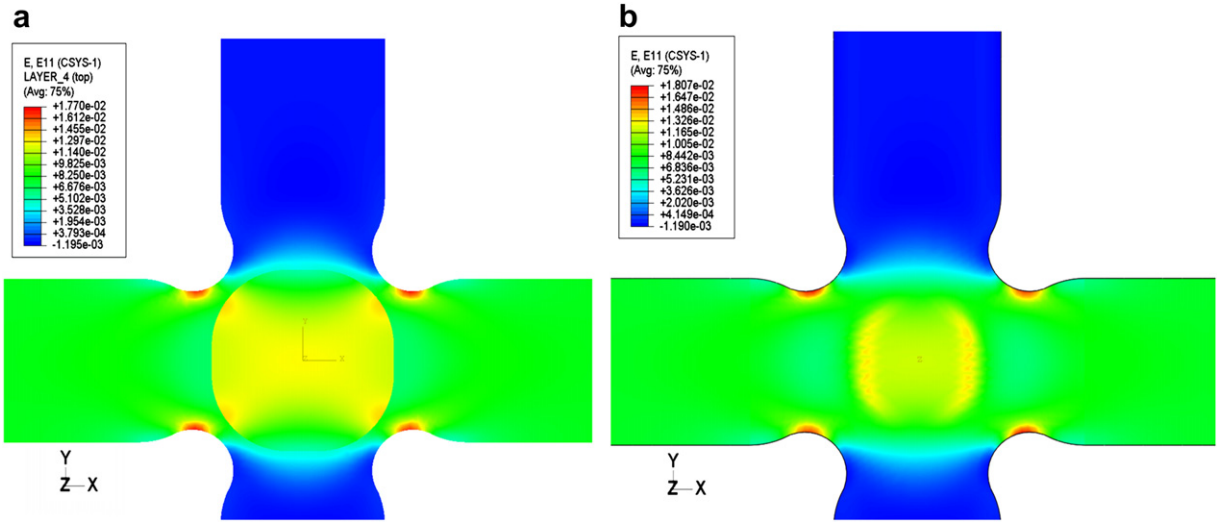

Fig. 7. Strain ε_{xx} in the first un-milled [+45°] layer for the 2D model (a) and the 3D model (b).

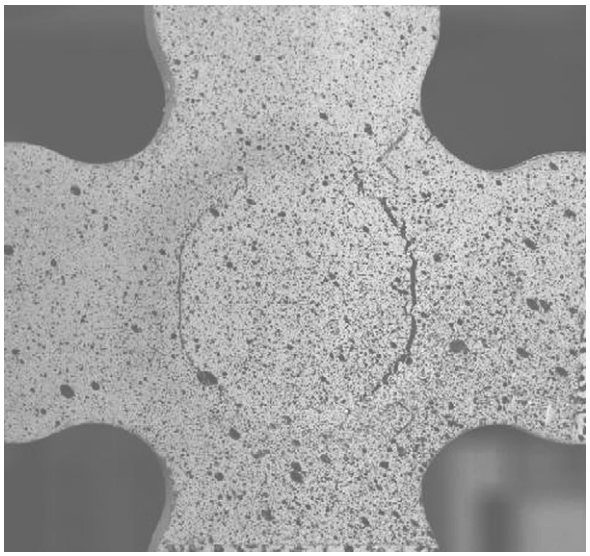

Fig. 8. Cracks initiated at the interface between the skew edges and the flat zone of the milled area.

a miscorrelation in the speckle pattern. As a result, the DIC method bridges this geometrical discontinuity in a numerical way by transforming the large displacements into high strains values. When these results are then compared with the linear elastic ones coming from the finite element model, a mismatch is, therefore, found due to the inability of the linear model to capture any discontinuity.

5. Conclusions

In this study, a mixed experimental/numerical approach, based on the finite element method and the digital image correlation technique, is presented to highlight the advantage of three-dimensional finite element models in comparison with two-dimensional ones in the investigation of biaxially loaded specimens. Despite the good results in and outside the central milled region for the two-dimensional model, a large difference remains in the vicinity of the geometrical discontinuities. Implementation of a three-dimensional model revealed that the experimentally obtained results were incorrect due to the initiation of cracks at the transition zone of these geometrical irregularities. This shows that the influence of discontinuities, such as the milled zone and the fillet corners, on the strain distribution can only be captured by more detailed three-dimensional models, whereas two-dimensional models are only reliable outside these regions.

Acknowledgements

The authors gratefully acknowledge the financial support for this research by the Fund for Scientific Research – Flanders (FWO).

References

[1] M. Quaresimin, Fatigue behaviour and life assessment of composite laminates under multiaxial loading, in: Proceedings of Fourth International Conference on Fatigue of Composites (ICFC4), Kaiserslautern, Germany, Europe, 2007.
[2] H. Nie, X. Qiao, W.X. Fan, A criterion for fatigue damage under combined bending and torsion based on the local stress–strain method. Fatigue and Fracture of Engineering Materials and Structures 15 (2) (1992) 225–227.
[3] D.l. McDiarmi, New analysis of fatigue under combined bending and twisting. Aeronautical Journal 78 (763) (1974) 325–329.
[4] H. Kakuno, Y. Kawada, New criterion of fatigue-strength of a round bar subjected to combined static and repeated bending and torsion. Fatigue of Engineering Materials and Structures 2 (2) (1979) 229–236.
[5] K.E. Atcholi, et al., Superposed torsion flexure of composite-materials – experimental-method and example of application. Composites 23 (5) (1992) 327–333.
[6] J.E. Bird, J.L. Duncan, Strain-hardening at high-strain in aluminum-alloys and its effect on strain localization. Metallurgical Transactions A-Physical Metallurgy and Materials Science 12 (2) (1981) 235–241.
[7] D. Lefebvre, et al., A high-strain biaxial-testing rig for thin-walled tubes under axial load and pressure. Experimental Mechanics 23 (4) (1983) 384–392.
[8] A. Zouani, T. Bui-Quoc, M. Bernard, Cyclic stress–strain data analysis under biaxial tensile stress state. Experimental Mechanics 39 (2) (1999) 92–102.
[9] J.P. Boehler, S. Demmerle, S. Koss, A new direct biaxial testing machine for anisotropic materials. Experimental Mechanics 34 (1) (1994) 1–9.
[10] A. Makinde, L. Thibodeau, K.W. Neale, Development of an apparatus for biaxial testing using cruciform specimens. Experimental Mechanics 32 (2) (1992) 138–144.
[11] J.S. Welsh, D.F. Adams, Development of an electromechanical triaxial test facility for composite materials. Experimental Mechanics 40 (3) (2000) 312–320.
[12] J.S. Welsh, D.F. Adams, An experimental investigation of the biaxial strength of IM6/3501-6 carbon/epoxy cross-ply laminates using cruciform specimens. Composites Part A-Applied Science and Manufacturing 33 (6) (2002) 829–839.
[13] Y. Yu, et al., Design of a cruciform biaxial tensile specimen for limit strain analysis by FEM. Journal of Materials Processing Technology 123 (1) (2002) 67–70.
[14] Optimat, reliable optimal use of materials for wind turbine rotor blades (acronym: OPTIMAT BLADES), in: Sixth Framework of the Specific Research and Technology Development Programme Energy, Environment and Sustainable Development with Contract Number ENK6-CT-2001-00552.
[15] D. Post, Moire interferometry at Vpi-and-Su. Experimental Mechanics 23 (2) (1983) 203–210.
[16] W.G. Gottenberg, Some applications of holographic interferometry. Experimental Mechanics 8 (9) (1968) 405.
[17] D.J. Chen, F.P. Chiang, Computer-aided speckle interferometry using spectral amplitude fringes. Applied Optics 32 (2) (1993) 225–236.